

Effects of dark matter on the inspiral properties of the binary neutron star

H. C. Das^{1,2,*}, Ankit Kumar^{1,2,†} and S. K. Patra^{1,2‡}

¹*Institute of Physics, Sachivalaya Marg, Bhubaneswar-751005, India and*

²*Homi Bhabha National Institute, Training School Complex, Anushakti Nagar, Mumbai 400094, India*

(Dated: April 6, 2021)

We study the properties of the binary neutron star (BNS) systems in the inspiral phase. To calculate the equation of state (EOS) of the neutron star (NS), we take the relativistic mean-field (RMF) model. The RMF model, namely NL3 (stiff) and two extended RMF model IOPB-I (less stiff) and G3 (soft) are taken to explore the properties of the NS. We assume that the dark matter (DM) particles are accreted inside the NS due to its enormous gravitational field. Different macroscopic properties of the NS such as mass M , radius R , tidal deformability λ and dimensionless tidal deformability Λ are calculated at different DM fractions. With the addition of DM inside the NS, the value of the quantities like M , R , λ and Λ decreases. To explore the BNS properties in the inspiral phase, the post-Newtonian (PN) formalism is considered because it is suitable up to the last orbits in the inspiral phase. We calculated the strain amplitude of the polarization waveforms h_+ and h_\times , $(2,2)$ mode waveform h_{22} , orbital phase Φ , frequency of the gravitational wave f and PN parameter x with DM as an extra candidate inside the NS. We find that the BNS with soft EOS sustains more time in their inspiral phase as compare to stiff EOS. In the case of DM admixed NS, the BNS with high DM fractions survives more time in the inspiral phase than lesser fraction of DM. The magnitude of f , Φ and x are almost the same for all the assumed parameter sets, but their inspiral time in the last orbit is different. We find a significant change in the BNS systems properties in the inspiral phase with DM inside the NS.

I. INTRODUCTION

The first detection of the binary neutron star (BNS) coalescence event GW170817 by LIGO/Virgo collaborations gives a new insight to study the compact objects [1, 2]. The gravitational wave (GW) instruments observed this event about 40 Mpc distance from the source with the total mass of $2.74 M_\odot$ [1]. Gamma rays are detected 1.7 seconds after the merger of the BNS [3, 4]. The optical telescopes identified an electromagnetic counterpart 12 hours after the GW event near the NGC 4993 galaxy called AT2017gfo [5–7]. The X-rays and radio waves were also detected several days after the merger [8–10]. Hence, the BNS collision event witnesses the beginning of a new era in multimessenger astronomy [11]. The GWs coming from the inspiral and merger of the compact binary stars are the most promising sources for ground-based detectors such as LIGO [12], Virgo [13] and KAGRA [14]. The GWs encodes the information about the tidal deformability of the BNS systems. The bound on the dimensionless tidal deformability Λ for the canonical star is given by GW170817, $\Lambda_{1.4} = 190_{-120}^{+390}$, which translates into a stringent bound $\Lambda \leq 580$ at the 90% confidence level [2]. Some work had been dedicated to constrain the mass M , radius R and Λ of the neutron star (NS) using the GW170817 data [15–20]. Hence, the tidal deformability is the most promising parameter to constrain the EOSs, M and R of the NS. The detailed study of the GWs emitting from the inspiral phase need an accurate theoretical framework. This is because the tidal effects influence late inspiral orbits dynamics and modify the corresponding gravitational waveforms. Different analysis had already done to study the properties of BNS systems, with

tidal interactions as dominant contributions in the late inspiral phase [21–28].

The post-Newtonian (PN) formalism is suitable up to the last orbit to study the BNS systems in the inspiral phase. The high accuracy PN template for the inspiral stage plays a key role in the GW science data analysis. The PN formalism re-expresses the general relativistic description of particles into the standard equations of motion, which express in terms of acceleration of the particles [29]. It is a slow-motion, weakly stressed, weak field approximation to the general theory of relativity and valid for any mass ratio, which are far away from each other [29, 30]. In the PN method, the equations of motion are found by systematically expanding the metric. The Einstein field equations are expressed in powers of the dimensionless parameter $\epsilon = \sqrt{GM/c^2 d} \sim \frac{v}{c}$, where M is the total mass of the system, d is the distance between two NS and v is the characteristic velocity of particles. The metric is then solved iteratively in powers of ϵ , and the equations of motion are evaluated from the metric using the geodesic equation. An expansion containing terms up to ϵ^n or equivalently $(1/c)^n$ is denoted an $\frac{n}{2}$ PN expansion [29, 31]. This calculation takes the energy and luminosity up to 3PN and 3.5PN order, respectively, for the inspiralling binary in quasi-circular orbits.

The BNS in its inspiral phase tidally interact with each other, which affects their stellar structure. Each star's tidal property depends on the macroscopic properties, such as M , R and second Love number k_2 which are all model-dependent [32]. Therefore, in this calculations we take a relativistic mean-field (RMF) model to calculate the NS's properties. Although, the standard RMF takes into account the self-interaction of the scalar (σ -mesons) it doesn't include any other self-meson coupling. By the inclusion of σ -meson self-coupling, the incompressibility approaches to the experimental range leaving unexplained the experimental flow data. The extended RMF (E-RMF) Lagrangian includes self and cross-couplings of the mesons up to fourth-order and predicted in-

* harish.d@iopb.res.in

† ankit.k@iopb.res.in

‡ patra@iopb.res.in

compressibility is well suited with the experimental value. The E-RMF model gives a good description of the finite nuclei and reproduces NS's properties as well [33, 34]. In this case, we take one standard RMF parameter set NL3 [35], and two E-RMF sets IOPB-I [34] and G3 [33] to calculate the properties of the NS with the dark matter as an extra candidate inside it.

Dark matter (DM) accounts for approximately 85% of the matter in the Universe and about 27% of its total mass-energy density. Theoretically, several DM particles have been hypothesised due to its unknown character such as weakly interacting massive particle (WIMPs) [36, 37], feebly interacting massive particles (FIMPs) [38, 39], Axions [40] etc. But WIMP is the most abundant DM particle, which is also considered as the thermal relics of the Universe. It might have decayed in the dense region of the Universe, which produce the standard model (SM) particles, leptons, gamma-rays and neutrinos at freeze-out temperature [41]. Direct and indirect detection experiments had already been established to know the mystery of DM [42–44]. Also, different models have been incorporated to study the effects of DM inside compact objects such as NS, and white dwarf [45–47]. The accretion of self-annihilating DM particles inside the NS affects the cooling properties [46, 48]. On the other hand, the non-annihilating DM particles develop interaction with baryons which affects the structure of the NS [49, 50]. In this model, we assume that the WIMP is a DM particle that is non-annihilating in character.

The addition of DM inside the NS generally reduces the microscopic properties such as M , R and λ [37, 51, 52]. This is because the EOS becomes softer with the increase of DM percentage. In the present case, we study the BNS properties in the inspiral phase for DM admixed NS. The emission of GWs and its properties such as the (2,2) mode waveform h_{22} , polarization waveforms h_+ & h_\times , GW frequency f , orbital phase Φ and PN parameter x are calculated for equal mass binary NS. We take three different RMF EOS to see the parametric dependence, spanning from soft to stiff. All the inspiral properties defined above are calculated in the retarded time interval. The distance between source and observer is 100 Mpc.

The manuscript is organized as follow: In Sec. II, we give the basic RMF formalism required for the calculation of NS properties with the admixture of DM inside the NS. In sub-sec. II A, we described the E-RMF formalism starting with E-RMF Lagrangian. Then, the EOSs are calculated using stress-tensor techniques. In sub-sec. II C, we briefly reported the interaction Lagrangian and the total EOS of the NS with the addition of DM. The detailed formalism can be found from our previous analysis [51, 52]. The inspiral phase of the BNS systems in quasi-circular orbits are detailed in sub-sec. II D. In Sec. III, we present our numerical results and descriptions in a consistent manner. Finally, we concluded our idea in Sec. IV. We use constants $G = c = 1$ in the gravitational unit system.

II. FORMALISM

A. Equation of state of the NS using RMF model

In the RMF model, the nucleons interact with each other by exchanging the mesons. Here, we considered σ , ω , ρ , and δ -mesons as the mediating particles. The symbolise for mesons masses and their fields are considered as standard and can be found in Refs. [33, 34]. The interaction Lagrangian is modelled by considering the self and cross-couplings of the mesons up to fourth-order [33, 34, 52]. The E-RMF Lagrangian for the nuclear matter (NM) system is [52, 53]

$$\begin{aligned} \mathcal{L}_{NM} = & \sum_{j=p,n} \bar{\psi}_j \left\{ \gamma_\mu \left(i\partial^\mu - g_\omega \omega^\mu - \frac{1}{2} g_\rho \vec{\tau}_j \cdot \vec{\rho}^\mu \right) - \left(M_{nucl.} \right. \right. \\ & \left. \left. - g_\sigma \sigma - g_\delta \vec{\tau}_j \cdot \vec{\delta} \right) \right\} \psi_j + \frac{1}{2} \partial^\mu \sigma \partial_\mu \sigma - \frac{1}{2} m_\sigma^2 \sigma^2 \\ & + \frac{\zeta_0}{4!} g_\omega^2 (\omega^\mu \omega_\mu)^2 - \frac{\kappa_3}{3!} \frac{g_\sigma m_\sigma^2 \sigma^3}{M_{nucl.}} - \frac{\kappa_4}{4!} \frac{g_\sigma^2 m_\sigma^2 \sigma^4}{M_{nucl.}^2} \\ & + \frac{1}{2} m_\omega^2 \omega^\mu \omega_\mu - \frac{1}{4} W^{\mu\nu} W_{\mu\nu} + \frac{\eta_1}{2} \frac{g_\sigma \sigma}{M_{nucl.}} m_\omega^2 \omega^\mu \omega_\mu \\ & + \frac{\eta_2}{4} \frac{g_\sigma^2 \sigma^2}{M_{nucl.}^2} m_\omega^2 \omega^\mu \omega_\mu + \frac{\eta_\rho}{2} \frac{m_\rho^2}{M_{nucl.}} g_\sigma \sigma \left(\vec{\rho}^\mu \cdot \vec{\rho}_\mu \right) \\ & + \frac{1}{2} m_\rho^2 \left(\vec{\rho}^\mu \cdot \vec{\rho}_\mu \right) - \frac{1}{4} \vec{R}^{\mu\nu} \cdot \vec{R}_{\mu\nu} \\ & - \Lambda_\omega g_\omega^2 g_\rho^2 (\omega^\mu \omega_\mu) (\vec{\rho}^\mu \cdot \vec{\rho}_\mu) + \frac{1}{2} \partial^\mu \vec{\delta} \partial_\mu \vec{\delta} - \frac{1}{2} m_\delta^2 \vec{\delta}^2 \quad (1) \end{aligned}$$

All coupling parameters constraint from the experimental data. The values of the coupling parameters are given in Table I. The saturation density is more for IOPB-I as compare to NL3 and G3. All the NM properties are well matches with the empirical/experimental data as given in Table I. The equations of motion for σ , ω , ρ and δ mesons have been calculated with mean-field approximations as given in the Refs. [33, 34, 53]. The energy density and pressure of the NM systems are calculated from the energy-momentum stress-tensor [54], which are given as follow

$$\begin{aligned} \mathcal{E}_{NM} = & \frac{\gamma}{(2\pi)^3} \sum_{j=p,n} \int_0^{k_j} d^3 k E_j^*(k_j) + \rho_b W + \frac{1}{2} \rho_3 R \\ & + \frac{m_s^2 \Sigma^2}{g_s^2} \left(\frac{1}{2} + \frac{\kappa_3}{3!} \frac{\Sigma}{M_{nucl.}} + \frac{\kappa_4}{4!} \frac{\Sigma^2}{M_{nucl.}^2} \right) \\ & - \frac{1}{2} m_\omega^2 \frac{W^2}{g_\omega^2} \left(1 + \eta_1 \frac{\Sigma}{M_{nucl.}} + \frac{\eta_2}{2} \frac{\Sigma^2}{M_{nucl.}^2} \right) \\ & - \frac{1}{2} \left(1 + \frac{\eta_\rho \Sigma}{M_{nucl.}} \right) \times \frac{m_\rho^2}{g_\rho^2} R^2 - \Lambda_\omega (R^2 \times W^2) \\ & - \frac{1}{4!} \frac{\zeta_0 W^4}{g_\omega^2} + \frac{1}{2} \frac{m_\delta^2}{g_\delta^2} D^2, \quad (2) \end{aligned}$$

TABLE I. The parameters are listed for three parameter sets. Except k_3 (fm^{-1}) all others are in dimensionless unit. The NM properties at the saturation density are given in the lower panel of the table in MeV unit except ρ_0 (fm^{-3}) and M^*/M (dimensionless). The empirical/experimental values are given in the last column with their Refs. [a] [55], [b] [56], [c] [57], [d] [58], [e] [59].

Parameter	NL3	G3	IOPB-I	Empirical/Expt. Value
$m_\sigma/M_{nucl.}$	0.541	0.559	0.533	0.426 – 0.745 [a]
$m_\omega/M_{nucl.}$	0.833	0.832	0.833	0.833 – 0.834 [a]
$m_\rho/M_{nucl.}$	0.812	0.820	0.812	0.825 – 0.826 [a]
$m_\delta/M_{nucl.}$	0.0	1.043	0.0	1.022 – 1.064 [a]
$g_\sigma/4\pi$	0.813	0.782	0.827	
$g_\omega/4\pi$	1.024	0.923	1.062	
$g_\rho/4\pi$	0.712	0.962	0.885	
$g_\delta/4\pi$	0.0	0.160	0.0	
κ_3	1.465	2.606	1.496	
κ_4	-5.688	1.694	-2.932	
ζ_0	0.0	1.010	3.103	
η_1	0.0	0.424	0.0	
η_2	0.0	0.114	0.0	
η_ρ	0.0	0.645	0.0	
Λ_ω	0.0	0.038	0.024	
ρ_0 (fm^{-3})	0.148	0.148	0.149	0.148-0.185 [b]
B/A	-16.29	-16.02	-16.10	-15.00–17.00 [b]
M^*/M	0.595	0.699	0.593	—
J	37.43	31.84	33.30	30.20-33.70 [c]
L	118.65	49.31	63.58	35.00-70.00 [c]
K_{sym}	101.34	-106.07	-37.09	-174–31 [d]
K	271.38	243.96	222.65	220-260 [e]

$$\begin{aligned}
P_{NM} = & \frac{\gamma}{3(2\pi)^3} \sum_{j=p,n} \int_0^{k_j} d^3k \frac{k^2}{E_j^*(k_j)} + \frac{1}{4!} \frac{\zeta_0 W^4}{g_\omega^2} \\
& - \frac{m_s^2 \Sigma^2}{g_s^2} \left(\frac{1}{2} + \frac{\kappa_3}{3!} \frac{\Sigma}{M_{nucl.}} + \frac{\kappa_4}{4!} \frac{\Sigma^2}{M_{nucl.}^2} \right) \\
& + \frac{1}{2} m_\omega^2 \frac{W^2}{g_\omega^2} \left(1 + \eta_1 \frac{\Sigma}{M_{nucl.}} + \frac{\eta_2}{2} \frac{\Sigma^2}{M_{nucl.}^2} \right) \\
& + \frac{1}{2} \left(1 + \frac{\eta_\rho \Sigma}{M_{nucl.}} \right) \frac{m_\rho^2}{g_\rho^2} R^2 + \Lambda_\omega (R^2 \times W^2) \\
& - \frac{1}{2} \frac{m_\delta^2}{g_\delta^2} D^2. \tag{3}
\end{aligned}$$

The Σ , W , R and D represents the redefined mesons fields for σ , ω , ρ and δ mesons respectively [52]. The term $E_j^*(k_j) = \sqrt{k_j^2 + M_j^2}$, where k_j represents the nucleons Fermi momenta and M_j is the effective masses of the nucleons. γ is the spin degeneracy factor whose value is 2 for individual nucleons.

B. Neutron star EOS

Inside the NS, the neutron decays to proton, electron and anti-neutrino. For the stability of the system, the inverse β -decay is also takes place to maintain both β equilibrium and charge neutrality. Hence, the EOS of NS calculated by taking contribution both from the nucleons and leptons. The NS's energy density and pressure are found to be [51, 52].

$$\begin{aligned}
& \mathcal{E}_{NS} = \mathcal{E}_{NM} + \mathcal{E}_l, \\
& \text{and} \quad P_{NS} = P_{NM} + P_l, \tag{4}
\end{aligned}$$

with,

$$\mathcal{E}_l = \sum_{l=e,\mu} \frac{2}{(2\pi)^3} \int_0^{k_l} d^3k \sqrt{k^2 + m_l^2}, \tag{5}$$

and

$$P_l = \sum_{l=e,\mu} \frac{2}{3(2\pi)^3} \int_0^{k_l} \frac{d^3k k^2}{\sqrt{k^2 + m_l^2}}. \tag{6}$$

Where \mathcal{E}_l , P_l and k_l are the energy density, pressure and Fermi momentum for leptons respectively.

C. Interaction of DM candidates in NS

Neutron stars, when evolved its lifetime in the Universe, the DM particles are accreted inside it due to its huge gravitational field and immense baryonic density [46, 60–62]. Here, we take Neutralino as a DM candidate, a super-symmetric particle and the best candidate of WIMP [51, 62–64]. The DM particles are interacting with nucleons by exchanging standard model (SM) Higgs. The detailed formalism and used notations can be found from our previous paper [51, 52]. The total Lagrangian is

$$\begin{aligned}
\mathcal{L} = & \mathcal{L}_{NM} + \bar{\chi} [i\gamma^\mu \partial_\mu - M_\chi + y h] \chi + \frac{1}{2} \partial_\mu h \partial^\mu h \\
& - \frac{1}{2} M_h^2 h^2 + f \frac{M_{nucl.}}{v} \bar{\psi} h \psi, \tag{7}
\end{aligned}$$

where \mathcal{L}_{NM} is the NM Lagrangian and ψ and χ are the nucleonic and DM wave functions respectively. The parameters y is DM-Higgs coupling, f is the nucleon-Higgs form factor and v is the vacuum expectation value of Higgs field. The values of y , f and v are 0.07, 0.35 and 246 GeV respectively taken from the Refs. [51, 52]. We constraint the values of y and f from both the direct/indirect detection experiments and LHC searches [52]. M_χ is the mass of the DM equal to 200 GeV as considered for this calculation. The energy density (\mathcal{E}) and pressure (P) for NS with DM can be calculated by solving the Eq. (7)

$$\mathcal{E} = \mathcal{E}_{NS} + \frac{2}{(2\pi)^3} \int_0^{k_f^{DM}} d^3k \sqrt{k^2 + (M_\chi^*)^2} + \frac{1}{2} M_h^2 h_0^2 \tag{8}$$

and

$$P = P_{NS} + \frac{2}{3(2\pi)^3} \int_0^{k_f^{DM}} \frac{d^3k k^2}{\sqrt{k^2 + (M_\chi^*)^2}} - \frac{1}{2} M_h^2 h_0^2 \quad (9)$$

where k_f^{DM} and M_χ^* are the Fermi momentum and the effective mass of DM respectively. M_h is the mass of the Higgs equal to 125 GeV, and h_0 is the Higgs field calculated by applying the mean-field approximation [62]. The contribution of the Higgs field in both energy density and pressure is minimal. The calculated \mathcal{E} and P are depicted in Fig. 1.

The NS's mass and radius are calculated by solving the Tolmann-Oppenheimer-Volkoff (TOV) equations and shown in Fig. 2. The NS is deformed when it is in the external field created by its companion star. The tidal deformability parameter ($\lambda = \frac{2}{3} k_2 R^5$) depends on the structural/macrosopic properties of the NS. The dimensionless k_2 can be calculated by solving two coupled differential equations as in Refs. [22, 32, 34]. The values of R and k_2 are fixed for a given mass by the EOS for the NS. The dimensionless tidal deformability Λ is defined as ($\Lambda = \lambda/M^5$). The calculated value of λ and Λ are presented in Fig. 3 for the IOPB-I parameter set with and without DM.

D. Binary neutron stars in quasi-circular orbits

1. PN-expanded Taylor-T4

Binary neutron stars emit GWs in their inspiral phases. The emission of GWs forces the system to move in quasi-circular orbits. The flux emitted by the system balances the rate of change of energy with time in that orbit. Therefore the energy balance equation is given as [31, 65, 66]

$$\mathcal{L} = -\frac{dE}{dt} = -\frac{dE/dx}{dt/dx}, \quad (10)$$

where E is the energy of the system, t is time, and x is the PN parameter which is defined as

$$x = \left(M_t \frac{d\Phi}{dt} \right)^{2/3} = \left(M_t \Omega \right)^{2/3}, \quad (11)$$

where M_t is the total mass of BNS systems, Φ is the orbital phase, Ω is the orbital angular velocity defined as $\Omega = 2\pi\omega$, ω is the orbital angular frequency, $\omega = f/2$, and f is the frequency of the emitted GWs. The energy of the system calculated up to 3PN order in terms of x is given as [29, 65, 66]

$$E = -\frac{1}{2} M_t \nu x \left\{ 1 + \left(-\frac{3}{4} - \frac{\nu}{12} \right) x + \left(-\frac{27}{8} + \frac{19\nu}{8} - \frac{\nu^2}{24} \right) x^2 + \left[-\frac{675}{64} + \left(\frac{34445}{576} - \frac{205\pi^2}{96} \right) \nu - \frac{155\nu^2}{96} - \frac{35\nu^3}{5184} \right] x^3 \right\} \quad (12)$$

where $\nu = m_1 m_2 / M_t^2$ is the symmetric mass ratio, m_1 and m_2 are the individual masses of the binary. The luminosity

\mathcal{L} is calculated by the time derivative of Eq. (12) using PN expansions up to 3.5 order is given as [29, 65, 66]

$$\mathcal{L} = \frac{32}{5} \nu^2 x^5 \left\{ 1 + \left(-\frac{1247}{336} - \frac{35\nu}{12} \right) x + 4\pi x^{3/2} + \left(-\frac{44711}{9072} + \frac{9271\nu}{504} + \frac{65\nu^2}{18} \right) x^2 + \left(-\frac{8191}{672} - \frac{583\nu}{24} \right) \pi x^{5/2} + \left[\frac{6643739519}{69854400} + \frac{16\pi^2}{3} - \frac{1712\gamma_E}{015} - \frac{856}{105} \ln(16x) + \left(-\frac{134543}{7776} + \frac{41\pi^2}{48} \right) \nu - \frac{94403\nu^2}{3024} - \frac{775\nu^3}{324} \right] x^3 + \left(-\frac{16285}{504} + \frac{214745\nu}{1728} + \frac{193385\nu^2}{3024} \right) \pi x^{7/2} \right\}, \quad (13)$$

where $\gamma_E \approx 0.5772$ is the Euler's constant. The phase evolution of the binary systems can be calculated by solving the following equations.

$$\frac{dx}{dt} = \frac{dE/dt}{dE/dx} = -\frac{\mathcal{L}}{dE/dx}, \quad (14)$$

$$\frac{d\Phi}{dt} = \frac{x^{3/2}}{M_t}. \quad (15)$$

There are several methods to integrate these systems of equations labelled as TaylorT1-TaylorT4 [31, 66, 67]. In the TaylorT1 method, the Eqs. (12) and (13) are inserted in Eq. (14) and then the integration is done using the initial conditions $x_0 = (M_t \Omega_0)^{2/3}$ and Φ_0 . In the TaylorT2 method, the equations are written by starting with a parametric solution of energy balance equations. Then, each expressions integrand is re-expanded as a single PN parameter x and truncated at the appropriate order [31, 66].

$$t(x) = t_0 + \int_x^{x_0} dx \frac{(dE/dx)}{\mathcal{L}}, \quad (16)$$

$$\Phi(x) = \Phi_0 + \int_x^{x_0} dx \frac{x^{3/2}}{M_t} \frac{(dE/dx)}{\mathcal{L}}. \quad (17)$$

In the present calculations, we take TaylorT4 approximations. In this method, the right-hand side of the Eq. (16) is re-expanded as a single series and truncated at 3.5PN order before doing the integration. After calculating x , t and Φ , one can know the properties related to inspiralling binaries for the point-particle system. But for the BNS case, the tidal interaction comes in to picture, which has major significance on the inspiral properties. Thus, we plot the GW's strain amplitude with and without tidal contribution for the IOPB-I parameter set as a representative EOS in Fig. 4. Without tidal interactions, the BNS systems sustain more time in their inspiral phase.

Therefore, we have to include the extra part of tidal interactions with this point-particle approximation. The motion of

the system is tidally interacting, which influences their internal structures. Also, the tidal interactions affect the evolution of the GW phase by a parameter λ . Hence, the BNS system's tidal contributions must be added on the right-hand side of Eq. (14), which is modified as [68–70]:

$$\frac{dx}{dt} = \frac{64\nu}{5M_t} x^5 \{F_{3.5}^{\text{Taylor}}(x) + F^{\text{Tidal}}(x)\}, \quad (18)$$

where $F_{3.5}^{\text{Taylor}}$ is PN-expanded expression for point-mass contributions using Taylor-T4 approximation, given by [31, 68–71]

$$\begin{aligned} F_{3.5}^{\text{Taylor}}(x) = & 1 - \left(\frac{743}{336} + \frac{11}{4}\nu \right) x + 4\pi x^{3/2} + \left(\frac{34103}{18144} \right. \\ & + \frac{13661}{2016}\nu + \frac{59}{18}\nu^2 \left. \right) x^2 - \left(\frac{4159}{672} + \frac{189}{8}\nu \right) \pi x^{5/2} \\ & + \left[\frac{16447322263}{139708800} - \frac{1712}{105}\gamma_E - \frac{56198689}{217728}\nu + \frac{541}{896}\nu^2 \right. \\ & \left. - \frac{5605}{2592}\nu^3 + \frac{\pi^2}{48}(256 + 451\nu) - \frac{856}{105}\ln(16x) \right] x^3 \\ & + \left(-\frac{4415}{4032} + \frac{358675}{6048}\nu + \frac{91495}{1512}\nu^2 \right) \pi x^{7/2}, \quad (19) \end{aligned}$$

and where F^{Tidal} is the tidal contribution given by [68, 69]

$$F^{\text{Tidal}}(x) = \sum_{I=1,2} F_{LO}(\chi_I) x^5 (1 + F_1(\chi_I)x), \quad (20)$$

with

$$F_{LO}(\chi_I) = 4\hat{k}_2^I \left(\frac{12 - 11\chi_I}{\chi_I} \right), \quad (21)$$

and

$$F_1(\chi_I) = \frac{4421 - 12263\chi_I + 26502\chi_I^2 - 18508\chi_I^3}{336(12 - 11\chi_I)}, \quad (22)$$

where

$$\hat{k}_2^I = k_2^I \left(\frac{\chi_I}{C_I} \right)^5 \quad I = 1, 2. \quad (23)$$

For equal-mass binary case, the mass fraction, $\chi_1 = \chi_2 = \chi = 1/2$ and the compactness, $C_1 = C_2 = C$.

2. Polarization waveforms

From the observational point of view, the GW detector detects the radiation in the direction of source. Therefore, the polarization waveforms are measured in the line-of-sight of

source can be expressed as in spherical co-ordinates $(R, \hat{\theta}, \hat{\phi})$ as [65, 72]

$$h_+(t) = \frac{4}{r} \mathcal{M}^{5/3} \omega^{2/3} \left(\frac{1 + \cos^2 \theta}{2} \right) \cos(2\omega t_{ret} + 2\phi), \quad (24)$$

and

$$h_\times(t) = \frac{4}{r} \mathcal{M}^{5/3} \omega^{2/3} \cos \theta \sin(2\omega t_{ret} + 2\phi),$$

where \mathcal{M} is the chirp mass defined as $\mathcal{M} = \nu^{3/5} M$. The amplitudes of the GW polarization with a fixed ω depends on the binary masses through \mathcal{M} . The \mathcal{M} can also be derived as $\mathcal{M} = \frac{(m_1 m_2)^{3/5}}{(m_1 + m_2)^{1/5}}$. It is measured by LIGO with a good precision as $\mathcal{M} = 1.188_{-0.002}^{+0.004} M_\odot$ [1]. If we see the orbit edge-on, $\theta = \pi/2$, then h_\times vanishes and the GW is linearly polarized. If we put, $\theta = 0$, then h_+ and h_\times have the same amplitude, but only difference is the phase and hence it is circularly polarized.

The polarization waveforms for an equal mass binary NS (EMBNS) systems along the z-axis (optimally oriented observer) calculated up to 2.5PN are given by [31, 73, 74]

$$\begin{aligned} h_+^{(z)} = & \frac{M_t}{2D} x \left(\cos 2\Phi \left\{ -2 + \frac{17}{4}x - 4\pi x^{3/2} + \frac{15917}{2880}x^2 \right. \right. \\ & \left. \left. + 9\pi x^{5/2} \right\} + \sin 2\Phi \left\{ \frac{59}{5}x^{5/2} \right\} \right), \quad (25) \end{aligned}$$

$$\begin{aligned} h_\times^{(z)} = & \frac{M_t}{2D} x \left(\sin 2\Phi \left\{ -2 + \frac{17}{4}x - 4\pi x^{3/2} + \frac{15917}{2880}x^2 \right. \right. \\ & \left. \left. + 9\pi x^{5/2} \right\} + \cos 2\Phi \left\{ -\frac{59}{5}x^{5/2} \right\} \right). \quad (26) \end{aligned}$$

The dominant (2,2) mode up to 3PN order is written as follow [66, 71, 75]

$$\begin{aligned} h_{22} = & -8\nu \sqrt{\frac{\pi}{5}} \frac{M_t}{D} e^{-2i\Phi} x \left\{ 1 + \left(-\frac{107}{42} + \frac{55\nu}{42} \right) x + 2\pi x^{3/2} \right. \\ & + \left(-\frac{2173}{1512} - \frac{1069\nu}{216} + \frac{2047\nu^2}{1512} \right) x^2 + \left[\frac{-107\pi}{21} + \left(\frac{34\pi}{21} \right. \right. \\ & \left. \left. - 24i \right) \nu \right] x^{5/2} + \left[\frac{27027409}{646800} - \frac{856\gamma_E}{105} + \frac{2\pi^2}{3} + \frac{428i\pi}{105} \right. \\ & \left. - \frac{428}{105} \ln(16x) + \left(\frac{41\pi^2}{96} - \frac{278185}{33264}\nu \right) - \frac{20261\nu^2}{2772} \right. \\ & \left. + \frac{11463\nu^3}{99792} \right] x^3 \left. \right\}, \quad (27) \end{aligned}$$

where D is the distance between source and observer taken as $D = 100$ Mpc in our calculations.

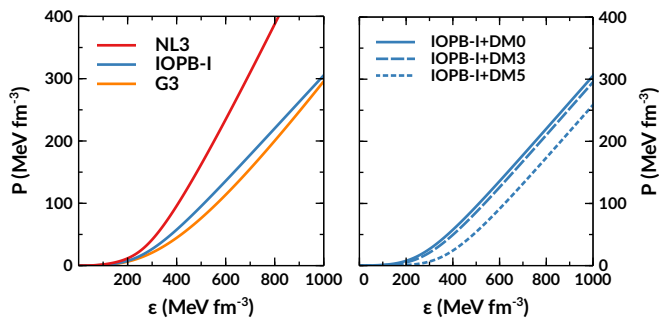


FIG. 1. (colour online) *Left*: EOSs are shown for 3-parameter sets NL3 (stiff), IOPB-I (less stiff) and G3 (soft). *Right*: The EOSs are shown with the addition of DM with $k_f^{DM} = 0, 0.03$ and 0.05 GeV for IOPB-I parameter set as representative case.

III. RESULTS AND DISCUSSIONS

A. EOS, mass-radius relation, tidal deformability

We take RMF EOS namely NL3 (stiff) [35], IOPB (less stiff) [34], and G3 (soft) [33] for the core part. The well known BCPM EOS [76] is used uniformly for all these sets to include the effect of the lower dense regions, i.e. the crust part and NS properties are calculated with unified EOS. We add the DM inside the NS, which interacts with nucleons via SM Higgs (see Sub-Sec. II C). For this, we take the IOPB-I parameter set as a representative EOS with $k_f^{DM} = 0, 0.03$ and 0.05 GeV, which are shortly written as IOPB-I+DM0¹, IOPB-I+DM3, and IOPB-I+DM5 respectively. The numerical values for $R_{1.35}, \lambda_{1.35}, \Lambda_{1.35}, k_{2,1.35}$ etc. for NS with mass $1.35 M_\odot$ are given in Table II. The predicted mass-radius of the NS for DM admixed NS with different DM momenta are also given for comparison. The maximum mass decreases with the increasing the k_f^{DM} . The total EOS of the NS is depicted in Fig. 1. From the right panel of Fig. 1, it is clear that with the increase of DM momentum, the EOS becomes softer, which is consistent with our previous results [51].

The M - R relation of a star is calculated by solving the TOV equations with EOS as the main input with the boundary conditions $P = P_c$ at $r = 0$ and $P = 0$ at $r = R$. The masses and radii with IOPB-I parameter sets are calculated for DM admixed NS, which are shown in Fig. 2. Recently measured massive pulsar PSR J0740+6620 [77], PSR J0348+0432 [78] and NICER [79, 80] results are also depicted. With the addition of DM, the maximum mass M_{max} and radius R_{max} decrease. For $k_f^{DM} = 0.03$ GeV, the M_{max} satisfy the constraint given by Cromartie *et al.* [77] as well as Antoniadis *et al.* [78] and radius constraint given by NICER [79, 80]. However, with $k_f^{DM} = 0.05$ GeV, the M_{max} and R_{max} become very less, which doesn't satisfy both massive pulsar and NICER data. Therefore, one can constraints the DM percentage inside the NS with the help of the observational data.

¹ same as IOPB-I because DM0 means no DM inside the NS

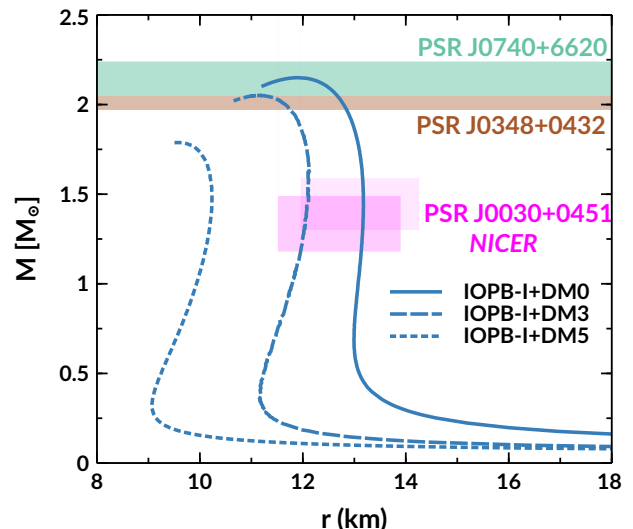


FIG. 2. (colour online) Mass-Radius plot for IOPB-I parameter sets with k_f^{DM} is equal to 0, 0.03 and 0.05 GeV. Recently measured heavy NS, PSR J0740+6620 [77] and PSR J0348+0432 [78] are shown with horizontal bars. The NICER results are also shown with two rectangles from two different analysis [79, 80].

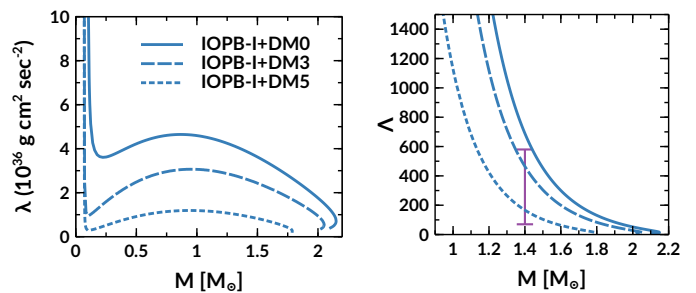


FIG. 3. (colour online) *Left*: The mass variation of tidal deformability of the NS is shown for IOPB-I set with two different DM momentum. *Right*: The dimensionless tidal deformability vs. masses of the NS with the addition of DM are shown. The vertical line with bar represents the GW170817 constraints on Λ .

The tidal deformability of the NS decreases with DM's addition, as shown in Fig. 3. The same trend also obtained for Λ . This is because, with the addition of DM, the EOS becomes softer and the mass and radius changes accordingly as shown in Fig. 2. Therefore, the softer EOS gives lower λ as compare to the stiffer one. The vertical double-headed line represents the constraints from GW170817 with, $\Lambda_{1.4} = 190_{-120}^{+390}$ [2]. The values of $\Lambda_{1.4}$ are 473.22, 169.644 for DM momentum 0.03 and 0.05 GeV respectively. Therefore, the value of $\Lambda_{1.4}$ with these DM momenta satisfies the constraints given by GW170817.

TABLE II. The maximum mass of the spherical NS M_{max} obtained with different EOS, the radius $R_{1.35}$, the tidal deformability $\lambda_{1.35}$, the dimensionless tidal deformability $\Lambda_{1.35}$, the tidal love number $k_{2,1.35}$, the compactness $C_{1.35}$ for NS mass $1.35 M_\odot$. The total mass of the BNS system's is $M_t = 2.7 M_\odot$ and $M_t \Omega_0 = M_t \pi f_0 = 0.0155$ are taken in this calculation with the minimum gravitational wave frequency $f_0 \approx 371$ Hz. $\lambda_{1.35}^*$ is in $10^{36} \text{ g cm}^2 \text{ sec}^{-2}$ unit.

EOS	$M_{max} (M_\odot)$	$R_{1.35} \text{ (km)}$	$\lambda_{1.35}^*$	$\Lambda_{1.35}$	$k_{2,1.35}$	$C_{1.35}$	$M_t \Omega_0$
NL3	2.775	14.568	7.415	1575.239	0.1130	0.137	0.0155
G3	1.979	12.476	2.754	585.182	0.0911	0.159	0.0155
IOPB-I	2.149	13.168	4.026	855.304	0.1017	0.151	0.0155
IOPB-I+DM3	2.051	12.047	2.717	577.237	0.1071	0.165	0.0155
IOPB-I+DM5	1.788	10.204	0.990	210.387	0.0896	0.195	0.0155

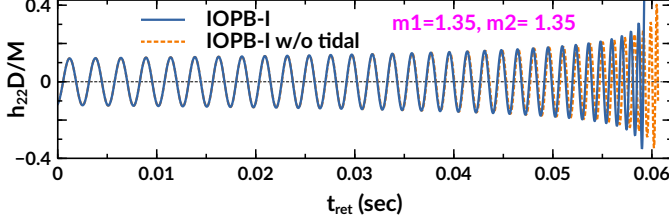


FIG. 4. (colour online) (2,2) mode waveforms are shown with and without tidal contributions for the IOPB-I parameter sets as a representative case.

B. Gravitational waves properties

In this sub-sec., we describe the BNS's inspiral properties using the PN formalism applied to quasi-circular orbit. These properties are calculated for EMBNS with three different parameter sets NL3, G3 and IOPB-I. For simplicity, we restrict our calculations only to EMBNS. We take IOPB-I as a representative EOS for the DM admixed NS since it predicts the mass of the NS $2.149 M_\odot$ which is consistent with PSR J0740+6620 [77]. Here, we calculate the polarization waveforms and the GW properties such as amplitude, frequency, phase for three different parameter sets. The properties are calculated at retarded time defined by [69]

$$t_{ret} = t - r_*, \quad (28)$$

where r_* is the tortoise coordinate defined as

$$r_* = r_A + 2M_t \ln \left(\frac{r_A}{2M_t} - 1 \right), \quad (29)$$

where $r_A = \sqrt{A/4\pi}$ with A is the proper surface area of the sphere. But for simplicity, the r_A is written as [69]

$$r_A = r \left(1 + \frac{M_t}{2r} \right)^2, \quad (30)$$

where $r \approx 200M_t$ is the finite spherical-coordinate radius.

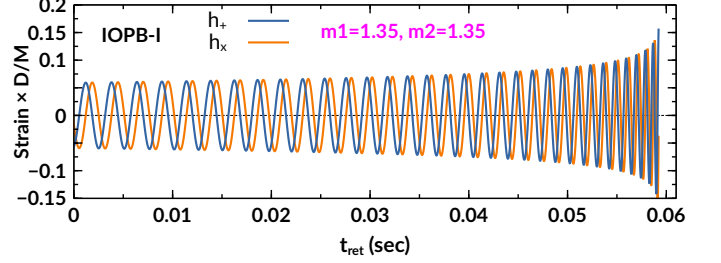


FIG. 5. (colour online) Plus and cross polarization waveforms are shown for the IOPB-I parameter sets.

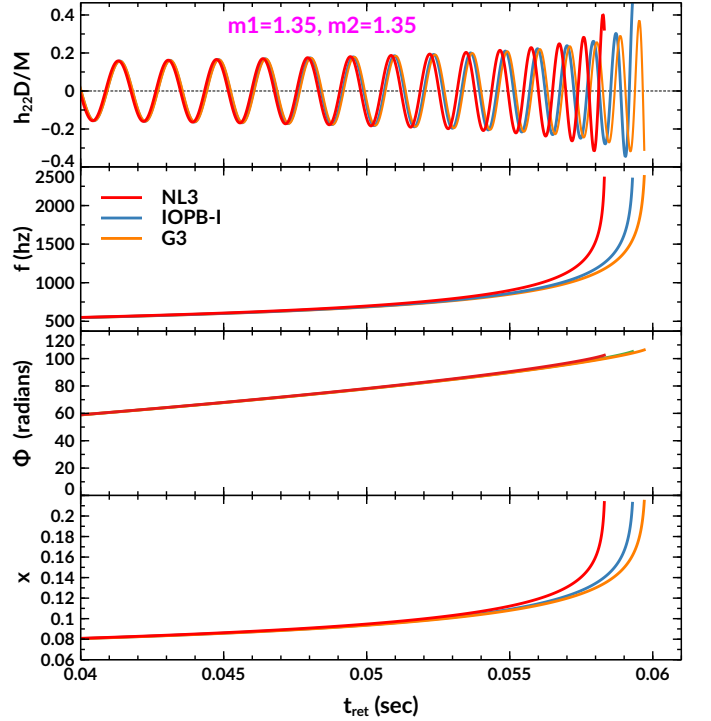


FIG. 6. (colour online) (2,2) mode waveform, frequency, phase and PN-parameters are shown for three parameter sets of the EMBNS in the retarded time interval calculated for $D = 100$ Mpc.

Fig. 6 shows the waveforms, frequencies, phases, and x for NL3, G3 and IOPB-I sets. The stiff EOS, like NL3, predicts higher mass and tidal deformability compared to the soft EOS

like G3. Therefore, the massive NS easily deformed by the presence of tidal fields created by its companion star. Hence, a less massive BNS system sustains a longer time than a more massive BNS system in the inspiral phase. This is because the tidal interactions accelerate the orbital evolution in the late inspiral phases due to increase in the interactions forces between two NSs. In Fig. 6, the topmost plot shows the (2,2) mode waveforms for three parameter sets. A careful inspection of the Fig. 6 indicates that the waveform corresponds to NL3 sustains less time than the other two IOPB-I and G3 sets in their inspiral phase. Similarly, different quantities like f , Φ and x are also shown for comparison.

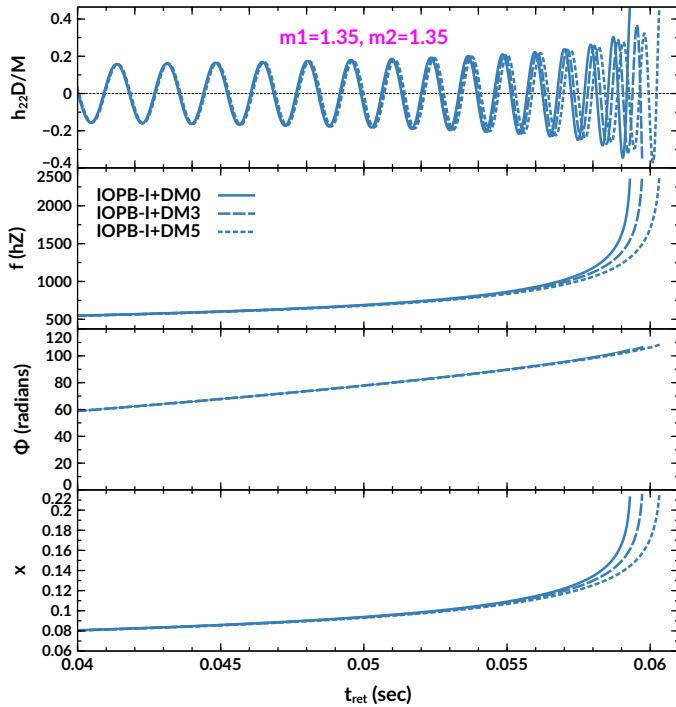


FIG. 7. (colour online) Same as Fig. 6, but for DM admixed NS with IOPB-I parameter set as a representative case.

With the addition of DM inside the NS, the inspiral properties such as h_{22} , f , Φ and x are changing significantly, shown in Fig. 7. The BNS with IOPB-I+DM5 sustains more time in the inspiral orbits as compare to IOPB-I+DM3. The magni-

tude of f , Φ and x are almost the same, but their inspiral time is different. Therefore, we conclude that DM has significant effects on inspiral properties.

IV. CONCLUSIONS AND REMARKS

We study the inspiral properties of the BNS system with the addition of DM inside the NS. To understand the NS EOS, we take the RMF formalism, which has large applications from finite nuclei to the astrophysical objects. The predictive competence of the RMF model is also discussed. We take three RMF EOS, such as NL3, IOPB-I and G3 to compare our numerical results. The EOS of the NS is calculated, which is the essential ingredient to solve the TOV equations. The M - R relations, tidal deformability λ and dimensionless tidal deformability Λ are calculated for three-parameter sets with and without DM taken into considerations. The adopted PN formalisms are briefly discussed, and their physical importance is also enumerated. In this study, we take only equal mass binary NS systems.

We compare the waveforms properties of the BNS systems in their inspiral phase with and without tidal interactions. We find that if the tidal interactions are switched-off, the BNS systems sustain more time in their inspiral phases. The polarization waveforms namely h_+ & h_\times and strain amplitude of h_{22} mode are calculated for three parameter sets. All the calculations are done in the retarded time interval with the distance between source and observer as 100 Mpc. We show that the systems with softer EOS such as G3 sustains more time than the stiffer EOS like NL3. Other properties such as frequencies, phases are almost identical in their magnitude. However, their inspiral time is different in the last orbits with different forces used.

The DM affects the NS's properties by assuming that the nucleons interacting with DM by SM Higgs. The coupling parameters are constrained from both direct/indirect detection and LHC searches. The macroscopic properties such as mass, radius, and tidal deformability decrease with the increase of DM percentage inside the NS. The inspiralling properties are also studied for the DM admixed NS. We find that with the addition of DM, the binary systems become less deformed, and it sustains more time in their inspiral phases. The other properties are also affected by the DM as compared to the normal matter. Hence, the DM effects on the inspiral properties of the BNS is significant.

[1] B. P. Abbott, R. Abbott, T. D. Abbott, *et al.* (LIGO Scientific Collaboration and Virgo Collaboration), *Phys. Rev. Lett.* **119**, 161101 (2017).
 [2] B. P. Abbott, R. Abbott, T. D. Abbott, *et al.* (The LIGO Scientific Collaboration and the Virgo Collaboration), *Phys. Rev. Lett.* **121**, 161101 (2018).
 [3] B. P. Abbott, R. Abbott, T. D. Abbott, F. Acernese, K. Ackley, C. Adams, T. Adams, P. Addesso, R. X. Adhikari, V. B. Adya, and *et al.*, *The Astrophysical Journal* **848**, L13 (2017).

[4] A. Goldstein, P. Veres, E. Burns, M. S. Briggs, R. Hamburg, D. Kocevski, C. A. Wilson-Hodge, R. D. Preece, S. Poolakkil, O. J. Roberts, and *et al.*, *The Astrophysical Journal* **848**, L14 (2017).
 [5] P. S. Cowperthwaite, E. Berger, V. A. Villar, B. D. Metzger, M. Nicholl, R. Chornock, P. K. Blanchard, W. Fong, R. Margutti, M. Soares-Santos, and *et al.*, *The Astrophysical Journal* **848**, L17 (2017).
 [6] M. Nicholl, E. Berger, D. Kasen, B. D. Metzger, J. Elias,

- C. Briceño, K. D. Alexander, P. K. Blanchard, R. Chornock, P. S. Cowperthwaite, and et al., *The Astrophysical Journal* **848**, L18 (2017).
- [7] R. Chornock, E. Berger, D. Kasen, P. S. Cowperthwaite, M. Nicholl, V. A. Villar, K. D. Alexander, P. K. Blanchard, T. Eftekhari, W. Fong, and et al., *The Astrophysical Journal* **848**, L19 (2017).
- [8] E. Troja, L. Piro, H. van Eerten, R. T. Wollaeger, M. Im, O. D. Fox, N. R. Butler, S. B. Cenko, T. Sakamoto, C. L. Fryer, and et al., *Nature* **551**, 71–74 (2017).
- [9] R. Margutti, E. Berger, W. Fong, C. Guidorzi, K. D. Alexander, B. D. Metzger, P. K. Blanchard, P. S. Cowperthwaite, R. Chornock, T. Eftekhari, and et al., *The Astrophysical Journal* **848**, L20 (2017).
- [10] G. Hallinan, A. Corsi, K. P. Mooley, K. Hotokezaka, E. Nakar, M. M. Kasliwal, D. L. Kaplan, D. A. Frail, S. T. Myers, T. Murphy, and et al., *Science* **358**, 1579–1583 (2017).
- [11] B. P. Abbott, R. Abbott, T. D. Abbott, et al., *The Astrophysical Journal* **848**, L12 (2017).
- [12] CALTECH, “LIGO Scientific Collaboration,” (2002).
- [13] INFN, “VIRGO Project Central Web site,” (1993).
- [14] KAGRA, “Kagra Observatory,” (2010).
- [15] B. Margalit and B. D. Metzger, *The Astrophysical Journal* **850**, L19 (2017).
- [16] D. Radice, A. Perego, F. Zappa, and S. Bernuzzi, *The Astrophysical Journal* **852**, L29 (2018).
- [17] N.-B. Zhang, B.-A. Li, and J. Xu, *The Astrophysical Journal* **859**, 90 (2018).
- [18] E. R. Most, L. R. Weih, L. Rezzolla, and J. Schaffner-Bielich, *Phys. Rev. Lett.* **120**, 261103 (2018).
- [19] R. Nandi, P. Char, and S. Pal, *Phys. Rev. C* **99**, 052802 (2019).
- [20] E. Annala, T. Gorda, A. Kurkela, and A. Vuorinen, *Phys. Rev. Lett.* **120**, 172703 (2018).
- [21] E. E. Flanagan and T. Hinderer, *Phys. Rev. D* **77**, 021502 (2008).
- [22] T. Hinderer, B. D. Lackey, R. N. Lang, and J. S. Read, *Phys. Rev. D* **81**, 123016 (2010).
- [23] J. Vines, E. E. Flanagan, and T. Hinderer, *Phys. Rev. D* **83**, 084051 (2011).
- [24] D. Bini, T. Damour, and G. Faye, *Phys. Rev. D* **85**, 124034 (2012).
- [25] J. S. Read, L. Baiotti, J. D. E. Creighton, J. L. Friedman, B. Giacomazzo, K. Kyutoku, C. Markakis, L. Rezzolla, M. Shibata, and K. Taniguchi, *Phys. Rev. D* **88**, 044042 (2013).
- [26] M. Favata, *Phys. Rev. Lett.* **112**, 101101 (2014).
- [27] L. Wade, J. D. E. Creighton, E. Ochsner, B. D. Lackey, B. F. Farr, T. B. Littenberg, and V. Raymond, *Phys. Rev. D* **89**, 103012 (2014).
- [28] M. Agathos, J. Meidam, W. Del Pozzo, T. G. F. Li, M. Tompitak, J. Veitch, S. Vitale, and C. Van Den Broeck, *Phys. Rev. D* **92**, 023012 (2015).
- [29] L. Blanchet, *Living Reviews in Relativity* **9**, 4 (2006).
- [30] A. Buonanno and B. S. Sathyaprakash, (2015), [arXiv:1410.7832 \[gr-qc\]](https://arxiv.org/abs/1410.7832).
- [31] M. Boyle, D. A. Brown, L. E. Kidder, A. H. Mroué, H. P. Pfeiffer, M. A. Scheel, G. B. Cook, and S. A. Teukolsky, *Phys. Rev. D* **76**, 124038 (2007).
- [32] T. Hinderer, *The Astrophysical Journal* **677**, 1216 (2008).
- [33] B. Kumar, S. Singh, B. Agrawal, and S. Patra, *Nuclear Physics A* **966**, 197 (2017).
- [34] B. Kumar, S. K. Patra, and B. K. Agrawal, *Phys. Rev. C* **97**, 045806 (2018).
- [35] G. A. Lalazissis, J. König, and P. Ring, *Phys. Rev. C* **55**, 540 (1997).
- [36] C. Kouvaris and P. Tinyakov, *Phys. Rev. D* **83**, 083512 (2011).
- [37] A. Quddus, G. Panotopoulos, B. Kumar, S. Ahmad, and S. K. Patra, *Journal of Physics G: Nuclear and Particle Physics* **47**, 095202 (2020).
- [38] L. J. Hall, K. Jedamzik, J. March-Russell, and S. M. West, *JHEP* **2010** (2010), [10.1007/jhep03\(2010\)080](https://arxiv.org/abs/1010.0780).
- [39] N. Bernal, M. Heikinheimo, T. Tenkanen, K. Tuominen, and V. Vaskonen, *IJMP A* **32**, 1730023 (2017).
- [40] L. D. Duffy and K. van Bibber, *New Journal of Physics* **11**, 105008 (2009).
- [41] F. Ruppin, J. Billard, E. Figueroa-Feliciano, and L. Strigari, *Phys. Rev. D* **90**, 083510 (2014).
- [42] R. Bernabei, P. Belli, F. Cappella, R. Cerulli, C. J. Dai, A. d’Angelo, H. L. He, A. Incicchitti, H. H. Kuang, J. M. Ma, and et al., *EPJ C* **56**, 333–355 (2008).
- [43] CDMS, *Science* **327**, 1619–1621 (2010).
- [44] E. Aprile, J. Aalbers, F. Agostini, M. Alfonsi, F. D. Amaro, M. Anthony, L. Arazi, F. Arneodo, C. Balan, P. Barrow, and et al., *Journal of Cosmology and Astroparticle Physics* **2016**, 027–027 (2016).
- [45] G. Bertone and M. Fairbairn, *Phys. Rev. D* **77**, 043515 (2008).
- [46] C. Kouvaris, *Phys. Rev. D* **77**, 023006 (2008).
- [47] C. Kouvaris and P. Tinyakov, *Phys. Rev. D* **82**, 063531 (2010).
- [48] S. A. Bhat and A. Paul, *The European Physical Journal C* **80**, 544 (2020).
- [49] A. De Lavallaz and M. Fairbairn, *Phys. Rev. D* **81**, 123521 (2010).
- [50] P. Ciarcelluti and F. Sandin, *Phys. Lett. B* **695**, 19–21 (2011).
- [51] H. C. Das, A. Kumar, B. Kumar, et al., *MNRAS* **495**, 4893 (2020).
- [52] H. C. Das, A. Kumar, B. Kumar, S. K. Biswal, and S. K. Patra, *Journal of Cosmology and Astroparticle Physics* **2021**, 007 (2021).
- [53] A. Kumar, H. C. Das, S. K. Biswal, B. Kumar, and S. K. Patra, *The European Physical Journal C* **80** (2020), [10.1140/epjc/s10052-020-8353-4](https://arxiv.org/abs/10.1140/epjc/s10052-020-8353-4).
- [54] N. K. Glendenning, *Compact stars: Nuclear physics, particle physics, and general relativity* (Springer-Verlag New York, 1997).
- [55] P. D. Group, P. A. Zyla, R. M. Barnett, et al., *Progress of Theoretical and Experimental Physics* **2020** (2020), [10.1093/ptep/ptaa104](https://arxiv.org/abs/10.1093/ptep/ptaa104), 083C01.
- [56] H. A. Bethe, *Annual Review of Nuclear Science* **21**, 93 (1971).
- [57] P. Danielewicz and J. Lee, *Nucl. Phys. A* **922**, 1 (2014).
- [58] J. Zimmerman, Z. Carson, K. Schumacher, A. W. Steiner, and K. Yagi, “Measuring nuclear matter parameters with nicer and ligo/virgo,” (2020), [arXiv:2002.03210 \[astro-ph.HE\]](https://arxiv.org/abs/2002.03210).
- [59] G. Colò, U. Garg, and H. Sagawa, *EPJ A* **50**, 26 (2014).
- [60] I. Goldman and S. Nussinov, *Phys. Rev. D* **40**, 3221 (1989).
- [61] Q.-F. Xiang, W.-Z. Jiang, D.-R. Zhang, and R.-Y. Yang, *Phys. Rev. C* **89**, 025803 (2014).
- [62] A. Das, T. Malik, and A. C. Nayak, *Phys. Rev. D* **99**, 043016 (2019).
- [63] S. P. Martin, “A Supersymmetry Primer,” in *Perspectives on Supersymmetry. Edited by KANE GORDON L. Published by World Scientific Publishing Co. Pte. Ltd* (1998) pp. 1–98.
- [64] G. Panotopoulos and I. Lopes, *Phys. Rev. D* **96**, 083004 (2017).
- [65] M. Maggiore, *Gravitational Waves: Volume 1: Theory and Experiments*, Gravitational Waves (OUP Oxford, 2008).
- [66] B. D. Lackey, *The Neutron-Star Equation of State and Gravitational Waves from Compact Binaries*, Ph.D. thesis (2012).
- [67] J. Creighton and W. Anderson, *Gravitational-Wave Physics and Astronomy: An Introduction to Theory, Experiment and Data Analysis*, Wiley Series in Cosmology (Wiley, 2011).

- [68] L. Baiotti, T. Damour, B. Giacomazzo, A. Nagar, and L. Rezzolla, *Phys. Rev. D* **84**, 024017 (2011).
- [69] K. Hotokezaka, K. Kyutoku, and M. Shibata, *Phys. Rev. D* **87**, 044001 (2013).
- [70] K. Hotokezaka, K. Kyutoku, Y.-i. Sekiguchi, and M. Shibata, *Phys. Rev. D* **93**, 064082 (2016).
- [71] L. Blanchet, G. Faye, B. R. Iyer, and S. Sinha, *Classical and Quantum Gravity* **25**, 165003 (2008).
- [72] S. Isoyama, R. Sturani, and H. Nakano, (2020), [arXiv:2012.01350 \[gr-qc\]](https://arxiv.org/abs/2012.01350).
- [73] K. G. Arun, L. Blanchet, B. R. Iyer, and M. S. S. Qusailah, *Classical and Quantum Gravity* **21**, 3771 (2004); [erratum-ibid](#) **22**, 3115 (2005).
- [74] L. E. Kidder, L. Blanchet, and B. R. Iyer, *Classical and Quantum Gravity* **24**, 5307 (2007).
- [75] L. E. Kidder, *Phys. Rev. D* **77**, 044016 (2008).
- [76] B. K. Sharma, M. Centelles, X. Viñas, M. Baldo, and G. F. Burgio, *A&A* **584**, A103 (2015).
- [77] H. T. Cromartie, E. Fonseca, S. M. Ransom, *et al.*, *Nature Astronomy* **4**, 72–76 (2019).
- [78] J. Antoniadis, P. C. C. Freire, N. Wex, *et al.*, *Science* **340** (2013), [10.1126/science.1233232](https://doi.org/10.1126/science.1233232).
- [79] M. C. Miller, F. K. Lamb, A. J. Dittmann, *et al.*, *APJ* **887**, L24 (2019).
- [80] T. E. Riley, A. L. Watts, S. Bogdanov, *et al.*, *APJ* **887**, L21 (2019).